Water Science and Engineering 2016, 9(1): 81−86

HOSTED BY

ELSEVIER

CrossMark

Available online at www.sciencedirect.com

Water Science and Engineering

journal homepage: http://www.waterjournal.cn

An experimental study on embankment failure induced by prolonged immersion in floodwater

Yu-long Luo*, Cheng Zhang, Min Nie, Mei-li Zhan, Jin-chang Sheng

College of Water Conservancy and Hydropower Engineering, Hohai University, Nanjing 210098, China

Received 12 April 2014; accepted 23 July 2014
Available online 7 November 2015

Abstract

Prolonged immersion in floodwater is one of the main causes of embankment failure or dam breaks, although failure mechanisms have not been extensively studied. In this study, an embankment model was constructed to investigate the influence of prolonged immersion in floodwater on the failure of an embankment. The results indicate that: (1) the phreatic surface gradually rises and negative pore pressures gradually dissipate with the time of prolonged immersion in floodwater, and, finally, a stable and fully saturated state is reached; (2) observable cracks and a heave phenomenon are found near the downstream toe and in the top stratum of the foundation, which are attributed to the large uplift pressure on the interface between the top stratum and the pervious substratum, the tremendous impact effect induced by the rapid rise in water level, and the reduction of shear strength of heavy silt loam. The present study enhances our in-depth knowledge of the mechanisms of embankment failure induced by floodwater, and provides experimental data for validation of mathematical models of the embankment seepage failure.

Keywords: Embankment; Floodwater; Seepage failure; Prolonged immersion; Heave phenomenon

1. Introduction

Prolonged immersion in floodwater is one of the main causes of embankment failure or dam breaks in the flood season. For example, the 1998 great flood in the Yangtze River Basin, lasting from late June to early July (Zong and Chen, 2000), caused damage to about 9396 main embankments of the Yangtze River, and economic losses were estimated at over US$ 36 billion (Ye and Glantz, 2005). The flood in New Orleans during Hurricane Katrina on August 29, 2005 caused levees and floodwalls to fail at more than 50 locations. Of the 284 miles of federal levees and floodwalls—there are approximately 350 miles in total—169 miles were damaged (Andersen et al., 2007). As a result, the problem of embankment failure induced by floodwater is a very important and urgent problem that should be studied in depth.

Generally, studies on seepage failure of the embankment have been mainly focused on two aspects: steady flow conditions and transient flow conditions. In examples of the former, Sellmeijer (1988) and Sellmeijer and Koenders (1991) developed an expression for the critical hydraulic head which should not be exceeded to avoid failure due to piping. Asaoka and Kodaka (1992) found that the critical hydraulic head difference in the medium-dense sand was more than three times as large as that in the loose sand. Ojha et al. (2003) presented a critical head model that provided a theoretical basis for Bligh's empirical model. Benmebarek et al. (2005) identified the conditions for seepage failure caused by boiling or heaving of the soil behind sheet piles. Fontana (2008) investigated critical hydraulic heads for the failure of hydraulic structures and assessed the coefficient of safety against heaving. Gregoretti et al. (2010) determined the minimum level of the upstream reservoir leading to the failure of landslide dams. Maknoon

This work was supported by the National Natural Science Foundation of China (Grant No. 51009053), the Priority Academic Program Development of Jiangsu Higher Education Institutions (Grant No. 3014-SYS1401), and the Program for Excellent Innovative Talents of Hohai University.
* Corresponding author.
E-mail address: lyl8766@hhu.edu.cn (Yu-long Luo).
Peer review under responsibility of Hohai University.

http://dx.doi.org/10.1016/j.wse.2015.11.001

and Mahdi (2010) found that the upstream water head did not have an important influence on the suffusion on the interface between the core and filter layers.

In examples of the latter, Ozkan (2003) and Ozkan et al. (2008) defined a sinusoidally varying boundary condition to simulate the changing water level, and studied the effects of transient flow and repetitive flood events. El Shamy and Aydin (2008) developed a three-dimensional fully coupled fluid-particle model, which can simulate the process of seepage failure of hydraulic structures due to a rapid rise in upstream water level. Awal et al. (2011) pointed out that the failure modes of landslide dams depend on the rate of water level rise in the upstream reservoir and the strength of the dam body. The experiment carried out by Luo et al. (2013) indicated that suffusion failure in transient flow conditions with the long-term large hydraulic head in the flood season was more likely to happen and much more serious than it is in steady conditions.

At present, seepage failure under transient flow conditions due to changes in the water level has not been analyzed in detail. Studies on steady flow are not consistent with actual conditions, because the typical flood conditions only act for a period of days to weeks, which may not be sufficient time to reach steady-state conditions. In studies on transient flow, the adverse influence of a rapid rise in water level has been considered, but the influence of prolonged immersion in floodwater on the seepage failure has not been extensively studied. Therefore, it is necessary to emphasize research on the mechanisms of the embankment failure induced by prolonged immersion in floodwater.

In this study, an embankment model was designed to investigate the influence of prolonged immersion in floodwater on seepage failure of the embankment. The variation of pore pressure, the evolution of the phreatic surface, and the seepage failure mode were analyzed.

2. Embankment failure experiment

2.1. Embankment model

The experiment was carried out in a glass-sided flume with a length of 3.75 m, a width of 0.5 m, and a height of 0.8 m. Water was fed into the flume through an attached upstream water tank and a glass plate with holes, used to prevent turbulence and produce a uniform flow. A schematic diagram of the embankment model is shown in Fig. 1. The embankment model was composed of 13 compaction layers with a height of each layer of 0.05 m (CLN1 to CLN13), of which CLN1 was constructed with sand, and CLN2 to CLN13 were constructed with heavy silt loam. The two types of soil are widely used for levee construction in China. The initial upstream and downstream slopes of the embankment were 1:1.3 and 1:1.2, respectively. Twenty pore pressure transducers were embedded at the preset positions to monitor the pore pressure over the whole process of the experiment. Table 1 shows the coordinates of all pore pressure transducers.

Fig. 2 depicts the grain size distributions of heavy silt loam and sand. The optimal water content, maximum dry density, and permeability of the heavy silt loam were 30%, 1.43 g/cm^3, and 1.04×10^{-6} cm/s, respectively, according to the normal laboratory experiments. The optimal water content, maximum dry density, and permeability of the sand were 12.36%, 1.5 g/cm^3, and 1.35×10^{-4} cm/s, respectively. Table 2 shows the soil-water characteristic relationships of the heavy silt loam and sand.

2.2. Experimental process

The experiment mainly contained the following six stages:

(1) Material preparation and compaction: A certain amount of material was mixed with sufficient water, and then, with the optimal water content, the mixture was compacted layer by layer. Heavy silt loam mud was smeared on the side wall of the flume before compaction to avoid seepage on the interface between the model and the side wall.

(2) Embedment of pore pressure transducers, as shown in Fig. 3: The transducers were embedded in the holes, and heavy silt loam mud was poured to ensure close contact between the transducers and the surrounding soil. Then, a certain amount of soil was added into the holes and compacted again. Because the scale of the transducers was very small in the context of the entire embankment model, the influence of transducers on the failure process was ignored.

(3) Discharge of air from the catheters of pore pressure transducers: Air entrapped in the catheters will influence the sensitivity of pore pressure transducers, so air discharge is

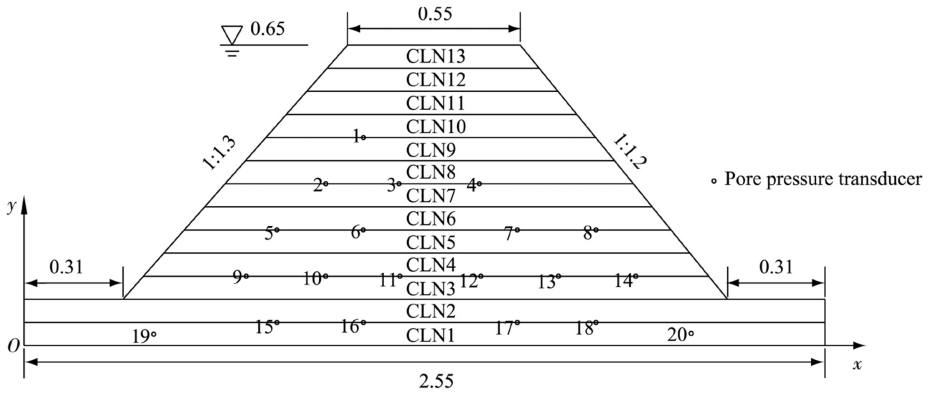

Fig. 1. Schematic diagram of embankment model (units: m).

Table 1
Coordinates of pore pressure transducers.

Number	x (m)	y (m)	Number	x (m)	y (m)
1	1.08	0.45	11	1.20	0.15
2	0.96	0.35	12	1.45	0.15
3	1.19	0.35	13	1.70	0.15
4	1.45	0.35	14	1.95	0.15
5	0.81	0.25	15	0.81	0.05
6	1.08	0.25	16	1.08	0.05
7	1.57	0.25	17	1.57	0.05
8	1.82	0.25	18	1.82	0.05
9	0.71	0.15	19	0.41	0.02
10	0.96	0.15	20	2.12	0.03

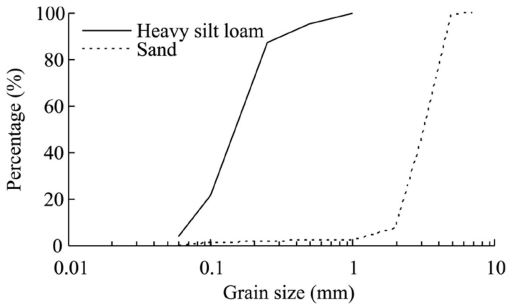

Fig. 2. Grain size distributions of heavy silt loam and sand.

significant. Distilled water was gradually injected into the catheters using an injector, and then the catheters were sealed when they were filled with water. Air discharge was conducted repeatedly, because the air in the unsaturated zone gradually entered the catheters throughout the process of the experiment.

(4) Calibration of the pore pressure transducers and monitoring of the initial seepage field in the embankment: The pore pressure transducers were calibrated by comparing the data from the pore pressure transducer with those of piezometric tubes.

(5) Rapid rise in the upstream water level: There was no water at the upstream and downstream of the embankments at first, and then the upstream water level rapidly rose to 0.65 m in 2 h.

Table 2
Soil-water characteristic relationship.

Matric suction (kPa)	Water content (%)		Matric suction (kPa)	Water content (%)	
	Heavy silt loam	Sand		Heavy silt loam	Sand
1.0	27.2	26.7	9.0	20.3	4.0
1.5	27.0	25.5	30.0	19.3	2.6
3.0	25.7	22.0	60.0	18.5	2.2
6.0	23.3	6.0	90.0	17.3	1.6

(6) Keeping the upstream high water level constant to simulate the prolonged duration of floodwater: The upstream water level was kept constant at 0.65 m until clear seepage failure appeared, and the pore pressure was recorded using the pore pressure transducers and data acquisition system.

3. Results and discussion

3.1. Variation of pore pressure

Fig. 4 shows the variation of pore pressure in stage 5 (time < 2 h) and stage 6 (time ≥ 2 h), where the negative pore pressure is referred to as matric suction. It can be seen from Fig. 4 that the variation of pore pressure is closely related to the position and time. The pore pressures rapidly increased during the period from 1 h to 6 h at transducers 2 and 3 next to the upstream boundary with an elevation of 0.35 m. The pore pressure at transducer 9 rapidly increased during the period from 0 to 2 h, which is mainly attributed to the rapid rise in the upstream water level. Sudden increases in the pore pressures at transducers 4, 8, and 14, which are mainly influenced by the seepage velocity in heavy silt loam and the prolonged duration of the high water level, were found at $t = 10$ h.

3.2. Evolution of phreatic surface

Fig. 5 shows the initial pore pressure head distribution before stage 5. The initial saturated zone is at the bottom of the embankment and the ratio of the area of the saturated zone to the total cross-sectional area (R_{st}) is only 5.84%. The

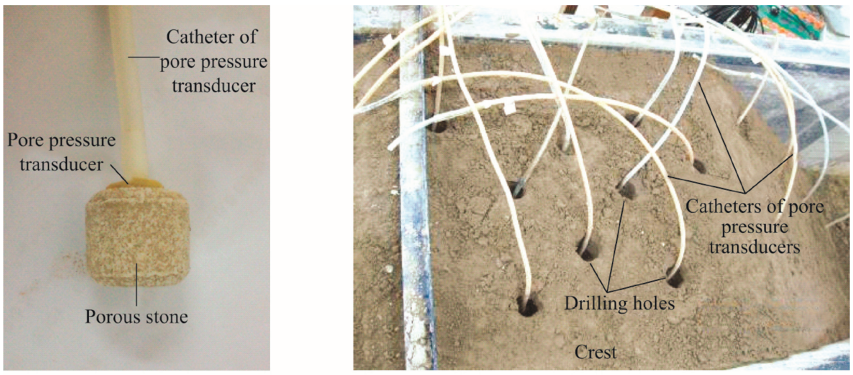

(a) Pore pressure transducer (b) Drilling hole

Fig. 3. Embedment of pore pressure transducers.

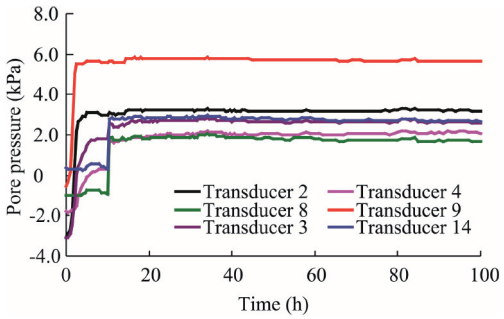

Fig. 4. Variations of pore pressure in embankment model.

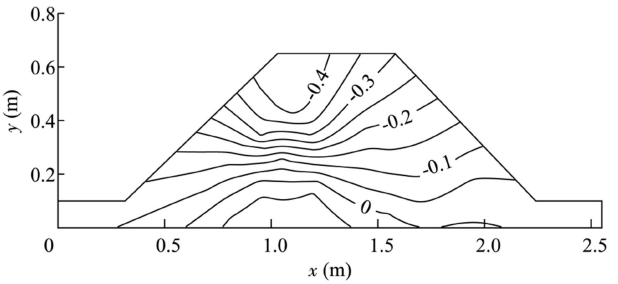

Fig. 5. Distribution of initial pore pressure head before stage 5 (units: m).

maximum value of negative pore pressure head is about −0.44 m, at the upstream crest.

The evolution of the phreatic surface (zero pore pressure head) in stage 6 is depicted in Fig. 6. It can be seen that the distribution of the pore pressure head in the embankment in stage 6 is very different from the way it is before stage 5. The phreatic surface and the elevation of the overflow point rose, and the matric suction decreased gradually with the time of prolonged immersion in floodwater. Fig. 7 shows the variation of the area of the saturated zone in the embankment at different times. At $t = 2$ h, the upstream zone of the embankment was saturated, the corresponding value of R_{st} was 30.2%, as shown in Fig. 7, and the maximum value of matric suction was located at the downstream crest. At $t = 5$ h, R_{st} reached 46.9%. At $t = 20$ h, the phreatic surface near the downstream toe rose rapidly, the overflow point was located at the downstream toe, and R_{st} increased to 68.1%. At $t = 50$ h, the elevation of the overflow point was 0.26 m, and R_{st} was 84.7%. At $t = 120$ h, the elevation of the overflow point reached 0.38 m, exceeding one half of the height of the embankment. The pore pressure heads in the embankment were all positive and a stable and fully saturated state was reached at $t = 240$ h. It can be seen that R_{st} increased rapidly from 5.8% to 68.1% during the first 20-h period. It should be pointed out that the evolution velocity of the area of the saturated zone is related to the permeability and compressibility of the heavy silt loam.

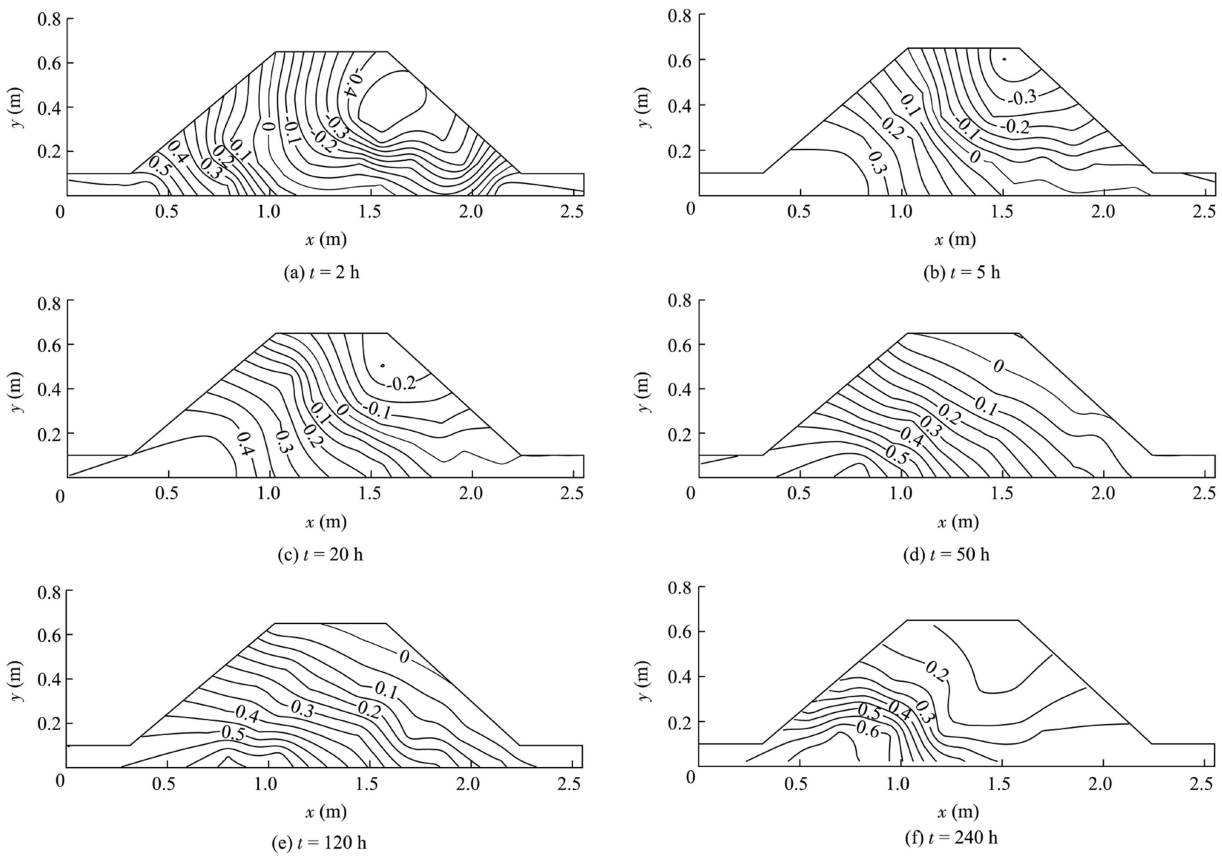

Fig. 6. Distribution of pore pressure head at different times in stage 6 (units: m).

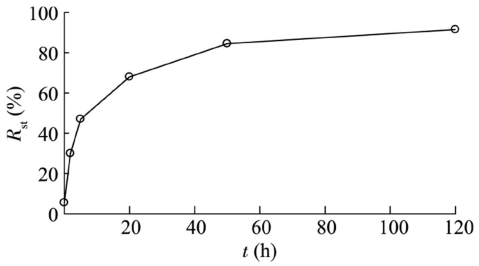

Fig. 7. Relationship between R_{st} and t.

3.3. Seepage failure mode

Fig. 8 shows the seepage failure mode at the downstream face of the embankment at $t = 50$ h and $t = 240$ h. At $t = 50$ h, some tiny cracks were found on the downstream face, and a little muddy water appeared on the top stratum (CLN2). At $t = 240$ h, some long and deep cracks formed an approximate circle slip surface, and much muddy water was entrapped on the top stratum.

Fig. 9 depicts the seepage failure mode in the downstream foundation of the embankment. At $t = 50$ h, a lot of layered and tiny cracks appeared near the downstream toe, which may be attributed to the increase in the uplift pressure on the interface between the top stratum (CLN2) and the pervious substratum (CLN1). At $t = 240$ h, a heave phenomenon was found near the downstream toe and in the top stratum, and interconnected cracks appeared in the heave region, as depicted in Fig. 9(b).

3.4. Discussion

The seepage failure of the embankment in this study may be attributed to the following factors:

(1) Large uplift pressures on the interface between the top stratum and pervious substratum: On the one hand, prolonged immersion in floodwater results in large pore pressures in the foundation. On the other hand, a large difference in permeability between the top stratum and pervious substratum gives rise to a large uplift pressure on their interface. If the uplift pressure on the interface is greater than the submerged weight of the top stratum, the excess pressure may cause heaving of the top stratum and result in concentrated flow failure.

For the embankment model in this study, the permeability of the top stratum and pervious substratum were 1.04×10^{-6} cm/s and 1.35×10^{-4} cm/s, and the corresponding ratio of the permeability was 1/127, so the water head difference was mainly undertaken by the top stratum. Simultaneously, the uplift pressure head on the interface between the two stratums reached 0.27 m at $t = 240$ h, and the corresponding uplift pressure exceeded the submerged weight of the top stratum. As a result, heave failure appeared.

(2) Tremendous impact effect induced by the rapid rise in water level: Luo et al. (2013) pointed out that the tremendous impact effect would increase the erosion power of seepage flow, partially destroy the structure of the soil skeleton, and

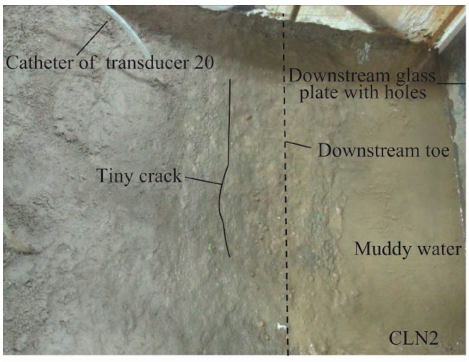

Fig. 8. Seepage failure mode at downstream face of embankment (top view).

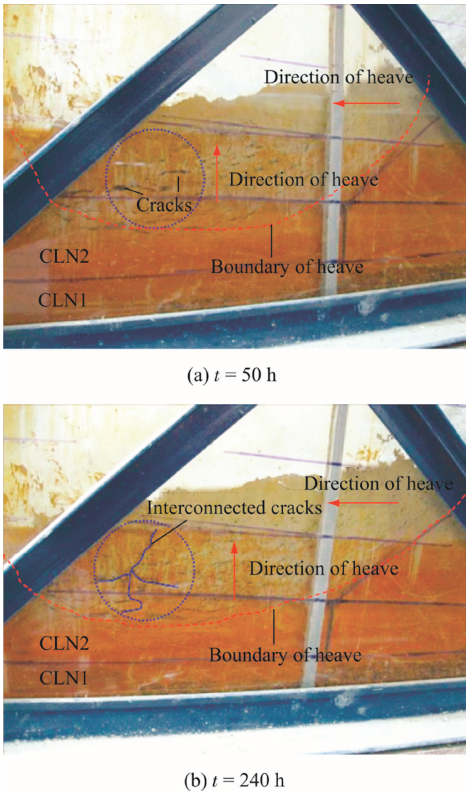

Fig. 9. Seepage failure mode in downstream foundation of embankment (front view).

significantly decrease the ability of the embankment to resist seepage failure.

For the embankment model in this study, the speed of the rise in the upstream water level reached 0.275 m/h, which was very fast for an actual project, so the induced impact effect was tremendous, and it was disadvantageous to seepage stability of the embankment.

(3) Reduction of shear strength: There are two factors influencing the shear strength: matric suction and prolonged immersion in floodwater. The shear strength decreases with the decrease in the matric suction; the prolonged immersion will cause soil particles to be fatter and softer, loosen the cementation of the soil particles, and then decrease the shear strength.

In this study, the matric suction gradually dissipated as the phreatic surface rose. In addition, the 10-d immersion also greatly weakened the shear strength of the heavy silt loam.

The ability of the embankment to resist seepage failure weakened owing to the above factors, and, finally, embankment failure appeared.

4. Conclusions

An embankment model was constructed to investigate the mechanism of the embankment failure induced by prolonged immersion in floodwater. Some conclusions can be drawn:

(1) The embankment failure occurring in the flood season is mainly attributed to the rapid rise in water level and the prolonged immersion in high water. The former induces a tremendous impact effect, which significantly decreases the resisting forces against seepage failure. The prolonged immersion leads to large uplift pressures at the bottom of the top stratum and the reduction of shear strength.

(2) The phreatic surface gradually rises and the negative pore pressures in the embankment gradually dissipate with the time of prolonged immersion in floodwater. Finally, a stable and fully saturated state is reached at $t = 240$ h.

(3) The seepage failure mode in this study is observable cracks and a heave phenomenon near the downstream toe and in the top stratum. The uplift pressure head on the interface between the top stratum and pervious substratum reaches 0.27 m at $t = 240$ h and the corresponding uplift pressure exceeds the submerged weight of the top stratum, which causes the heave phenomenon of the top stratum and results in concentrated flow along the cracks.

These results enhance our in-depth knowledge of the mechanisms of embankment failure induced by floodwater, and provide new experimental data for validation of mathematical models of the embankment seepage failure.

It should be pointed out that the experimental results are related to the compaction of the embankment, materials used for construction of the embankment, experimental procedures, etc. These factors will be studied in the future. In addition, new numerical models should be developed to make some comparisons between numerical and experimental results.

References

Andersen, C.F., Battjes, J.A., Daniel, D.E., Edge Jr., B., Espey, W., Gilbert, R.B., Jackson, T.L., Kennedy, D., Mileti, D.S., Mitchell, J.K., et al., 2007. The New Orleans Hurricane Protection System: What Went Wrong and Why? American Society of Civil Engineers, Reston.

Asaoka, A., Kodaka, T., 1992. Seepage failure experiments and their analyses of loose and medium dense sands. Soils Found. 32(3), 117−129. http://dx.doi.org/10.3208/sandf1972.32.3_117.

Awal, R., Nakagawa, H., Fujita, M., Kawaike, K., Baba, Y., Zhang, H., 2011. Study on piping failure of nature dam. Annuals of Disas. Prev. Res. Inst., Kyoto Univ. (54B), 539−546. http://dx.doi.org/10.2208/jscejhe.67.I_157.

Benmebarek, N., Benmebarek, S., Kastner, R., 2005. Numerical studies of seepage failure of sand within a cofferdam. Comput. Geotech. 32(4), 264−273. http://dx.doi.org/10.1016/j.compgeo.2005.03.001.

El Shamy, U., Aydin, F., 2008. Multiscale modeling of flood-induced piping in river levees. J. Geotech. Geoenviron. Eng. 134(9), 1385−1398. http://dx.doi.org/10.1061/(ASCE)1090-0241(2008)134:9(1385).

Fontana, N., 2008. Experimental analysis of heaving phenomena in sandy soils. J. Hydraul. Eng. 134(6), 794−799. http://dx.doi.org/10.1061/(ASCE)0733-9429(2008)134:6(794).

Gregoretti, C., Maltauro, A., Lanzoni, S., 2010. Laboratory experiments on the failure of coarse homogeneous sediment natural dams on a sloping bed. J. Hydraul. Eng. 136(11), 868−879. http://dx.doi.org/10.1061/(ASCE)HY.1943-7900.0000259.

Luo, Y.L., Qiao, L., Liu, X.X., Zhan, M.L., Sheng, J.C., 2013. Hydro-mechanical experiments on suffusion under long-term large hydraulic heads. Nat. Hazards 65(3), 1361−1377. http://dx.doi.org/10.1007/s11069-012-0415-y.

Maknoon, M., Mahdi, T.F., 2010. Experimental investigation into embankment external suffusion. Nat. Hazards 54(3), 749−763. http://dx.doi.org/10.1007/s11069-010-9501-1.

Ojha, C.S.P., Singh, V.P., Adrian, D.D., 2003. Determination of critical head in soil piping. J. Hydraul. Eng. 129(7), 511−518. http://dx.doi.org/10.1061/(ASCE)0733-9429(2003)129:7(511).

Ozkan, S., 2003. Analytical Study on Flood Induced Seepage Under River Levees. Ph.D. Dissertation. Louisiana State University, Baton Rouge.

Ozkan, S., Adrian, D.D., Sills, G.L., Singh, V.P., 2008. Transient head development due to flood induced seepage under levees. J. Geotech. Geoenviron. Eng. 134(6), 781−789. http://dx.doi.org/10.1061/(ASCE)1090-0241(2008)134:6(781).

Sellmeijer, J.B., 1988. On the Mechanism of Piping Under Impervious Structures. Delft University of Technology, Delft.

Sellmeijer, J.B., Koenders, M.A., 1991. A mathematical model for piping. Appl. Math. Model. 15(11−12), 646−651. http://dx.doi.org/10.1016/S0307-904X(09)81011-1.

Ye, Q., Glantz, M.H., 2005. The 1998 Yangtze Floods: The use of short-term forecasts in the context of seasonal to interannual water resource management. Mitig. Adapt. Strateg. Glob. Change 10(11), 159−182. http://dx.doi.org/10.1007/s11027-005-7838-7.

Zong, Y.Q., Chen, X.Q., 2000. The 1998 flood on the Yangtze, China. Nat. Hazards 22(2), 164−184. http://dx.doi.org/10.1023/A:1008119805106.